

Spin- and charge-density oscillations in spin chains and quantum wires

Stefan Rommer

Department of Physics and Astronomy, University of California, Irvine, California 92697

Sebastian Eggert

Institute of Theoretical Physics, Chalmers University of Technology and Göteborg University, 41296 Göteborg, Sweden

(Submitted: December 7, 1999. Last change: June 8, 2018)

We analyze the spin- and charge-density oscillations near impurities in spin chains and quantum wires. These so-called Friedel oscillations give detailed information about the impurity and also about the interactions in the system. The temperature dependence of these oscillations explicitly shows the renormalization of backscattering and conductivity, which we analyze for a number of different impurity models. We are also able to analyze screening effects in one dimension. The relation to the Kondo effect and experimental consequences are discussed.

PACS numbers: 71.10.Pm, 75.10.Jm, 72.15.Qm, 73.23.-b

I. INTRODUCTION

There is growing interest in impurities in low-dimensional electron and magnetic systems spurred by high temperature superconductivity and experimental progress in producing ever smaller electronic structures. There appears to be two central aspects that are studied most in this context, namely the effect of impurities on the transport properties in mesoscopic systems on the one hand,¹ and impurity-impurity interactions in antiferromagnetic systems due to impurity induced magnetic order² on the other hand. In this paper we show that the charge- and spin-densities near impurities give a great deal of information about both of those aspects and allow us to study a number of impurity models in one dimension in detail.

Induced density fluctuations at twice the Fermi wave-vector, so-called Friedel oscillations,³ are a common impurity effect in fermionic systems, which are enhanced in lower dimensions. There are two distinct physical effects that can give rise to Friedel oscillations. The most common source is a simple *interference effect* as considered in the original work by Friedel.³ Fermions scatter off the impurity, resulting in a superposition of incoming and outgoing wave-functions. Summing up the squares of the corresponding wave-functions up to the sharp cutoff at the Fermi wave-vector k_F results in a characteristic interference pattern with a $2k_Fx$ modulation, namely the Friedel oscillations. Clearly, this pattern can give a great deal of information about the impurity, in particular details about the scattering process. A second source for the $2k_Fx$ oscillations are *interaction effects* due to the screening of an impurity with a net charge or a magnetic moment. A typical example of this effect is the Kondo screening cloud,⁴ which we also analyze in this paper. The $2k_Fx$ oscillations due to screening have typically a different characteristic amplitude as a function of x than those due to backscattering, as we will discuss in more detail below.

We now consider the density oscillations in one-

dimensional systems such as spin-chains and interacting quantum wires (Luttinger Liquids) in order to understand the detailed effects of impurity scattering and screening as a function of temperature. In the classic work by Kane and Fisher^{1,5} it was found that a generic impurity in a spinless Luttinger Liquid results in a renormalization of the conductivity with temperature, which leads to a perfectly reflecting barrier at $T = 0$ for repulsive interactions. Interestingly, this behavior can also be explained in terms of repeated scattering off the Friedel oscillations, which gives an explicit expression of the transmission coefficient in the weak coupling limit.⁶ Independently, the analogous renormalization behavior was also found in the spin-1/2 chain,⁷ where a generic perturbation in the chain effectively renormalizes to an open boundary condition as $T \rightarrow 0$. However, it is possible that a special symmetry in the Hamiltonian reverses this renormalization, which leads to resonant tunneling in quantum wires^{5,8} or the healing of a two-link problem in the spin-1/2 chain.⁷ The renormalization behavior in that case is analogous to the two-channel Kondo effect.^{7,9}

The renormalization flow can easily be tested numerically by examining the scaling of the finite size energy gaps,^{7,10} but we now would like to determine the reflection coefficient directly by analyzing the induced density oscillations which are also interesting in their own right. In addition, we also consider the density oscillations from impurity models near an edge, impurities with a net charge or magnetic moment (Kondo-type impurities), and integrable impurities. The detailed renormalization of the impurity backscattering as well as screening can be studied in each case by analyzing the induced density oscillations as a function of temperature, which we determined numerically with the Transfer Matrix Renormalization Group (TMRG) for impurities.^{9,11,12} This allows us to make predictions for conductivity measurements in quantum wires and for Knight shift measurements in spin chains, e.g. Nuclear Magnetic Resonance (NMR) experiments. In all cases we find a typical renormalization to a fixed point of the Luttinger Liquid model,

which is described in terms of a simple (open or periodic) boundary condition in agreement with field theory calculations.

The rest of this paper is organized as follows. In Sec. II we present the model Hamiltonian and review the results for Friedel oscillations due to an open end (i.e. complete backscattering). Different impurity models of a modified link, two modified links, an edge impurity, Kondo impurities, and an integrable impurity are then analyzed in detail in Sec. III. Section IV contains a description of the numerical methods used and a critical discussion about the possible numerical errors. We conclude with a summary and a discussion about experimental relevance in Sec. V.

II. THE MODEL

The standard model we are considering here are spinless interacting fermions on a one-dimensional lattice, described by the Hamiltonian

$$H = \sum_i \left[-t(\Psi_i^\dagger \Psi_{i+1} + \Psi_{i+1}^\dagger \Psi_i) + Un_i n_{i+1} - \mu n_i \right], \quad (1)$$

where $n_i = \Psi_i^\dagger \Psi_i$ is the fermion density. Although this Hamiltonian neglects the spin degrees of freedom of real electrons in quantum wires, it captures the essential physics in conductivity experiments. Moreover, this model is equivalent to the spin-1/2 chain

$$H = \sum_i \left[\frac{J}{2}(S_i^+ S_{i+1}^- + S_i^- S_{i+1}^+) + J_z S_i^z S_{i+1}^z - BS_i^z \right] \quad (2)$$

where the spin operators are related to the fermion field by the Jordan-Wigner transformation

$$S_i^z = n_i - \frac{1}{2}, \quad S_i^- = (-1)^i \Psi_i \exp i\pi \sum_j^{i-1} n_j, \quad (3)$$

with $J = 2t$, $J_z = U$ and $B = \mu - U$.

The model in Eq. (1) can be analyzed by standard bosonization techniques in the low-temperature limit. For low energies we only consider excitations around the Fermi-points $\pm k_F$ and introduce left- and right-moving fermion fields with a linear dispersion relation

$$\Psi(x) = e^{-ik_F x} \psi_L(x) + e^{ik_F x} \psi_R(x). \quad (4)$$

The chiral fermion fields can then be bosonized using the usual bosonization rules

$$\psi_{L/R}^\dagger \psi_{L/R} = \frac{1}{\sqrt{4\pi}} (\partial_x \phi \pm \Pi_\phi), \quad (5)$$

where Π_ϕ is the conjugate momenta to the boson field ϕ . This results in the following boson Hamiltonian density

$$\mathcal{H} = \frac{v}{2} [g^{-1}(\partial_x \phi)^2 + g \Pi_\phi^2], \quad (6)$$

which can be solved by a simple rescaling of the boson with the interaction parameter g . The parameter g and the velocity v can in principle be calculated for any interaction strength U and chemical potential μ with Bethe ansatz techniques.¹³ To lowest order in U we get $g = 1 - 2U/\pi v$ and $v = \sqrt{4t^2 - \mu^2} + 2U/\pi$, so that $g < 1$ for repulsive interactions.

We now want to analyze the density oscillations using this formalism. Already from the decomposition of the fermion field in Eq. (4) it is clear that the fermion density may contain an oscillating component with $2k_F x$. To see this explicitly we can write the charge density in quantum wires (or equivalently the spin density $\langle S_z \rangle$ in spin chains) in terms of left- and right-movers

$$\begin{aligned} \langle \Psi^\dagger \Psi \rangle = & \langle \psi_L^\dagger \psi_L \rangle + \langle \psi_R^\dagger \psi_R \rangle \\ & + e^{i2k_F x} \langle \psi_L^\dagger \psi_R \rangle + e^{-i2k_F x} \langle \psi_R^\dagger \psi_L \rangle. \end{aligned} \quad (7)$$

The first two uniform terms just represent the overall fermion density in the bulk system, while the last two “Friedel” terms are the density oscillations n_{osc} we are interested in. In a system with translational invariance the left- and right-moving fields are uncorrelated $\langle \psi_L^\dagger \psi_R \rangle = 0$ and no density oscillations are present. An impurity, however, scatters left- into right-movers and the amplitude of the oscillations gives detailed information about the backscattering.

As the simplest example of this effect, let us consider an open boundary, i.e. an impurity with complete backscattering at the origin. In this case the correlation functions can be calculated directly.^{7,14–18} For the particular case of the left-right correlation function at equal space and time we find

$$\langle \psi_L^\dagger(x) \psi_R(x) \rangle \propto \left(\frac{\pi T}{v \sinh 2\pi x T/v} \right)^g, \quad (8)$$

so that the density oscillations are given by

$$n_{\text{osc}} \propto \sin(2k_F x) \left(\frac{\pi T}{v \sinh 2\pi x T/v} \right)^g. \quad (9)$$

The Friedel oscillations are exponentially damped with temperature, because the incoming and outgoing wavefunctions that form the interference pattern lose coherence due to temperature fluctuations. In the limit $T \rightarrow 0$ we recover the result of Ref. 19 where a power-law decay of the Friedel oscillation $n_{\text{osc}} \propto 1/x^g$ was predicted.

It is now important to realize that the fermions or spins are still pinned to a lattice, i.e. $x = \text{Integer}$, which gives interesting additional effects. In particular, at half-filling $k_F = \pi/2$ the Friedel oscillations in Eq. (9) are identically zero $\sin(\pi x) = 0$ for integer x , which can easily be understood from particle-hole symmetry (or equivalently spin-flip symmetry). Half-filling is a natural state for the spin chains in zero magnetic field, but a small magnetic

field changes the Fermi vector slightly $k_F = \pi/2 + B/v$. In that case, Eq. (9) becomes

$$n_{\text{osc}} \propto (-1)^x \sin(2Bx/v) \left(\frac{\pi T}{v \sinh 2\pi xT/v} \right)^g. \quad (10)$$

Now, the Friedel oscillations are simply alternating on the lattice and for distances below the magnetic length scale $x < v/B$ we can use $\sin(2Bx/v) \rightarrow 2Bx/v$ so that remarkably the oscillations actually *increase* with x^{1-g} . This effect was first observed for the Heisenberg chain ($J_z = J$, $g = 1/2$, $v = J\pi/2$), where the local susceptibilities $\chi(x)$ can be written as¹⁷

$$\chi(x) = \chi_0 - c (-1)^x \chi^{\text{bs}}(x), \quad (11)$$

with the amplitude of the alternating part given by

$$\chi^{\text{bs}}(x) = \frac{x\sqrt{T}}{\sqrt{\sinh 4xT}}. \quad (12)$$

Here χ_0 is the bulk susceptibility in the chain²⁰ and we measure T in units of J . The sign was chosen so that the (constant) overall amplitude c of the alternating part is positive. The superscript bs indicates that the alternating susceptibility is due to backscattering. As shown in Fig. 1 from TMRG simulations there is a characteristic maximum because the temperature damping eventually dominates over the increasing oscillations. Clearly, the expression in Eq. (12) reproduces the shape of this alternating part rather well, although we have neglected possible logarithmic corrections (multiplicative and additive), which may be responsible for the apparent shift in the characteristic maximum in Fig. 1. The numerical TMRG results of the local susceptibility near the open end $\chi^{\text{bs}}(x)$ will be used as the reference data for a completely backscattering impurity in our studies in the next section. The numerical data automatically contains all corrections due to irrelevant higher order operators. The logarithmic corrections to Eq. (12) due to the leading irrelevant operator have a special behavior near a boundary,²¹ which we have not tried to predict for the local susceptibility, but numerically we find that a possible multiplicative logarithmic correction for $\chi(x)$ appears to have a *negative* power of $\ln(x)$. The maximum in Fig. 1 occurs at $x \propto 1/T$ with an amplitude $\chi_{\text{alt}} \propto 1/\sqrt{T}$, which results in a characteristic feature in NMR experiments, so that it was possible to confirm this effect experimentally as well.²² At zero temperature the ground state has a staggered magnetization which has a maximum in the center of a finite chain (assuming an odd number of sites).²³ The magnetization for finite chains with impurities has also recently been analyzed, which resulted in interesting patterns that reveal the nature of the strong correlations in the system.²⁴

Even for a partially reflecting impurity we expect that the same alternating contribution as in Eq. (12) due to backscattering is present, but with an amplitude c that

increases monotonically with the reflection coefficient R . In fact we can make a firm connection between the relative amplitudes and the reflection coefficients by considering free fermions $U = 0$ for which we can find the eigenfunctions exactly even in the presence of impurities. Clearly the eigenfunctions are given by plane wave solutions $|k\rangle$ which contain a special mix of left- and right-moving components due to the impurity. Just like without impurities there are in fact always two such degenerate orthogonal solutions. We found the solutions for generic impurity models and looked at the spatial structure of the square of the wave-functions, which contains an interference pattern of incoming and outgoing waves. In general, we always find

$$|\langle x|k\rangle|^2 = \frac{1}{\pi} \left(1 + \sqrt{R(k)} \cos(2kx + 2\Phi) \right), \quad (13)$$

where the summation over the two degenerate solutions is implied. Here $R(k)$ is the ordinary k -dependent reflection coefficient which has been determined independently according to text-book methods. Therefore, the magnitude of the interference is exactly given by the square root of the reflection coefficient, which is maybe not too surprising but very useful in our analysis. In particular, when we consider the fermion density at half filling we are really directly looking at the spatial structure of the wave-function. We can write near half-filling (i.e. for a small field B in the spin chain model)

$$\begin{aligned} n(x) - 1/2 &= \int_{\pi/2}^{\pi/2+B/v} |\langle x|k\rangle|^2 dk \\ &\stackrel{B \rightarrow 0}{=} \frac{B}{v} \left| \langle x|\frac{\pi}{2} \rangle \right|^2 \\ &= B [\chi_0 - c_R (-1)^x \chi^{\text{bs}}], \end{aligned} \quad (14)$$

where we have used the fact that the spin density for the Heisenberg chain in a small field is just given by the susceptibility in Eq. (11), but with a coefficient c_R which now depends on the reflection coefficient R near half filling. Together with Eq. (13) we therefore arrive at the central result that at half-filling *the reflection coefficient is proportional to the square of the alternating density amplitude*

$$R = \left(\frac{c_R}{c} \right)^2, \quad (15)$$

where $c = c_{R=1}$ is the coefficient corresponding to complete backscattering in Eq. (11). We use this formula to estimate the reflection coefficient from the density oscillations for various impurity models in the following.

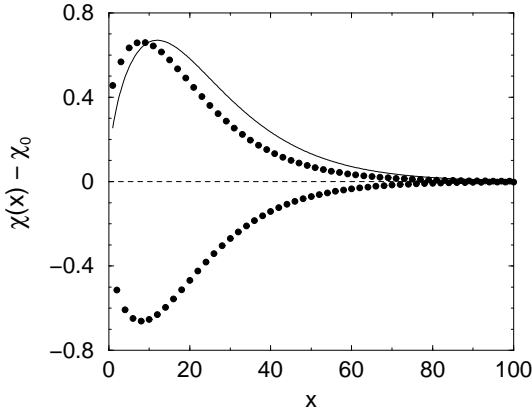


FIG. 1. Local susceptibility close to the open end of a spin-1/2 chain from TMRG data for $T = 0.04J$ compared to Eqs. (11) and (12) with $c = 0.51$, which was determined by matching the characteristic maxima.

As mentioned above there may also be $2k_Fx$ density oscillations due to screening, so that the alternating susceptibility is in general a sum of two parts

$$\chi^{\text{alt}}(x) \equiv \chi(x) - \chi_0 = (-1)^x [\chi^{\text{screening}}(x) - c_R \chi^{\text{bs}}(x)]. \quad (16)$$

In the case of overscreening the neighboring spins (or electrons) overcompensate the magnetic (or electric) impurity and leave an effective impurity with opposite moment which in turn gets screened by the next nearest neighbors and so on. This finally results in a screening cloud. Screening is purely an interaction effect where a $2k_Fx$ density oscillation is induced by an “active” impurity Hamiltonian $\langle \psi_L^\dagger \psi_R H_{\text{imp}} \rangle \neq 0$. The $2k_Fx$ oscillations due to backscattering, however, are purely an interference effect and are even present in non-interacting fermion systems. The special shape and the increasing nature of the alternating part in Eq. (12) for $g = 1/2$ makes it possible to easily identify the contribution due to backscattering, so that we can always separate the two possible effects near half-filling. In what follows we therefore always use the special choice of coupling $U = 2t$ corresponding to the Heisenberg model $J_z = J$. This model can be used to demonstrate the generic behavior of impurity effects in mesoscopic systems and also gives experimental consequences for spin-chain compounds. The Luttinger Liquid parameter takes the value $g = 1/2$ in this case, which is the strongest possible interaction at half-filling before Umklapp scattering becomes relevant.

III. IMPURITY MODELS

A. One modified link

Maybe the simplest impurity to consider is a weak link in the chain, i.e. a modified hopping J' between two sites in the chain as shown in Fig. 2

$$H = -t \sum_{i \neq 0} (\Psi_i^\dagger \Psi_{i+1} + \Psi_{i+1}^\dagger \Psi_i) - J' (\Psi_0^\dagger \Psi_1 + \Psi_1^\dagger \Psi_0). \quad (17)$$

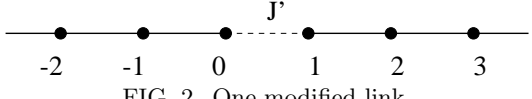


FIG. 2. One modified link.

The wave-functions and reflection coefficient $R(k)$ for this problem can be calculated exactly, with the result that

$$R(k) = \frac{t^4 - 2t^2 J'^2 + J'^4}{t^4 - 2t^2 J'^2 \cos 2k + J'^4}. \quad (18)$$

However, once the interaction U is introduced this problem becomes highly non-trivial and the reflection coefficient renormalizes with temperature T . The interacting system has been studied in the context of both spinless fermions¹ and the spin-1/2 chain,⁷ where it was found that repulsive interactions $U > 0$ make the perturbation of one link relevant, so that it renormalizes to a completely reflecting barrier as $T \rightarrow 0$. A small weakening of a link $J' \lesssim t$ produces a relevant backscattering operator in the periodic chain of scaling dimension $d = g$, so that this link effectively weakens further as the temperature is lowered. Below a cross-over temperature T_K (analogous to a Kondo-temperature) the link has weakened so much that it is more useful to consider the problem of two open ends that are weakly coupled, which is now described by an irrelevant operator of scaling dimension $d = 1/g$. Therefore, this coupling weakens further and ultimately the open boundary condition represents the stable fixed point as $T \rightarrow 0$. The same analysis is also true for a slight strengthening of a link $J' \gtrsim t$, because in this case the two ends lock into a “singlet” state as the effective coupling grows, and the remaining ends are weakly coupled with a virtual coupling of order t^2/J' which is again irrelevant.

We consider the interacting system with $U = 2t$, which we can write in terms of an SU(2) invariant spin Hamiltonian via the Jordan-Wigner transformation in Eq. (3) with a modified Heisenberg coupling between two spins

$$H = J \sum_{i \neq 0} \mathbf{S}_i \cdot \mathbf{S}_{i+1} + J' \mathbf{S}_0 \cdot \mathbf{S}_1. \quad (19)$$

We now want to analyze the density oscillation near the impurity in order to extract the reflection coefficient as described above. In Fig. 3 we show the amplitude of the alternating spin density for different coupling strengths J' . Clearly the shape as a function of distance x remains largely the same as in Fig. 1 for all J' so that the functional dependence in Eq. (12) is still adequate, but with an overall coefficient c which is now related to the reflection coefficient R as postulated in Eq. (15).

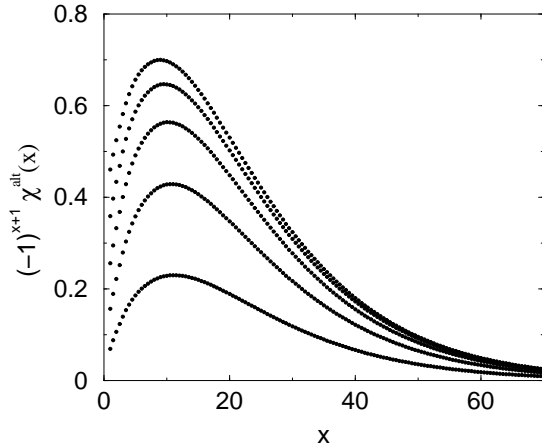


FIG. 3. Envelope of the alternating susceptibility of the one-link impurity at $T = 0.04J$ for $J'/J = 0.0, 0.2, 0.4, 0.6, 0.8$ from above.

The reflection coefficient is directly related to the renormalization behavior above. The basic idea behind renormalization is to use an effective Hamiltonian with renormalized parameters as a function of T . To estimate the reflection coefficient it is therefore possible to make a simplified but intuitive analysis by using the free fermion result in Eq. (18), but with a renormalized coupling strength $\tilde{J}'(T)$. Below the cross-over temperature $T < T_K$, the effective potential is small and given by the renormalization behavior of the leading irrelevant operator $\tilde{J}'(T) \propto J'T^{1/g-1}$. This results in

$$1 - R \propto J'^2 T^{2/g-2}, \quad (20)$$

which is the universal behavior near the stable fixed point as first predicted in Ref. 1. Above the cross-over temperature $T > T_K$ the renormalization behavior is better described by a relevant operator on the periodic chain giving $J - \tilde{J}'(T) \propto (J - J')T^{g-1}$. From this result it would even seem that we can recover the periodic chain in the high temperature limit, but it is of course important to realize that the renormalization is no longer possible above a cutoff of order J . For an initial bare coupling $J' \sim J$ very close to the unstable fixed point $T_K \ll J$ we therefore find that the effective coupling stops renormalizing at its bare value $\tilde{J}' \rightarrow J'$ for large T . In summary, the temperature dependence above T_K is not as universal as in Eq. (20), but we may still write

$$R \propto (J - J')^2, \quad (21)$$

for $J' \sim J$ and $T > T_K$.

It is now straightforward to extract the relative coefficient c_R/c in Eq. (14) from the numerical data by simply dividing the amplitude of the alternating part for each coupling J' in Fig. 3 by the reference data of χ^{bs} for the open chain. According to Eq. (15) the square of this relative coefficient then gives the reflection coefficient. Fig. 4 shows the results for the temperature dependent reflection coefficient from our TMRG data. The renormalization to a perfectly reflective barrier can clearly be seen

as $T \rightarrow 0$. The behavior for couplings close to the periodic fixed point ($J' \gtrsim 0.4J$) is consistent with Eq. (21). For smaller couplings the cross-over temperature T_K is larger, and we see an extended region where the scaling of the stable fixed point with J'^2 and $T^{2/g-2}$ in Eq. (20) holds (here $g = 1/2$). We can also compare our results to the findings of Matveev *et al* in Ref. 6 where an explicit formula for the transmission coefficient was given $1 - R \propto [(D/T)^{2\alpha} R_0 / (1 - R_0) + 1]^{-1}$ in terms of the non-interacting reflection coefficient R_0 in Eq. (18), a cut-off D , and a *small* interaction parameter $\alpha = 1/g - 1$. Unfortunately, the interaction parameter is large in our case $\alpha = 1$ so that this formula does not quantitatively agree with our findings in Fig. 4. Qualitatively, their result looks rather similar, but we observe a sharper renormalization at low temperatures near the unstable fixed point ($J' \gtrsim 0.4J$). Indeed we find that the region where the famous scaling in Eq. (20) is valid turns out to be extremely narrow for $J' \gtrsim 0.4J$.

Another aspect is the high temperature behavior where the non-interacting reflection coefficient in Eq. (18) should be approached⁶. This is indeed the case near the unstable fixed point $J' \gtrsim 0.4J$ where the non-interacting value is quickly reached with high accuracy. However, near the stable fixed point ($J' \lesssim 0.4J$) we find that the reflection coefficient can renormalize even well below the non-interacting value, so that the interactions actually *enhance* the conductivity at higher temperatures in this case. The reason for this unexpected behavior is that the cross-over temperature is larger than the cut-off near the stable fixed point $T_K \gg J$, so that the renormalization may continue beyond the bare coupling constants at higher temperatures.

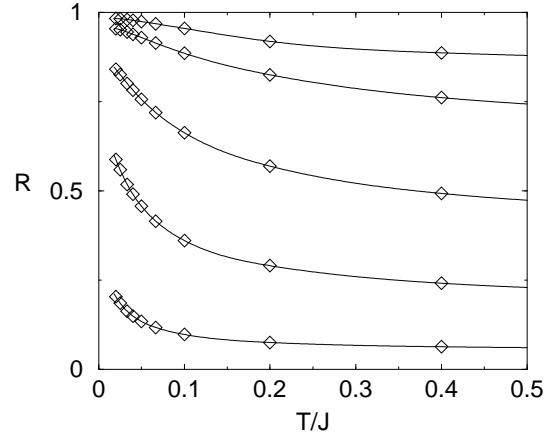


FIG. 4. Reflection coefficient R of one modified link for $J'/J = 0.1, 0.2, 0.4, 0.6, 0.8$ from above. The lines are guides for the eye.

B. Two modified links

We now consider the impurity of *two* neighboring modified links in the chain as shown in Fig. 5. For the in-

teracting case $U = 2t$ we can again write this model in terms of a Heisenberg spin chain model

$$H = J \sum_{i \neq -1,0} \mathbf{S}_i \cdot \mathbf{S}_{i+1} + J' \mathbf{S}_0 \cdot (\mathbf{S}_{-1} + \mathbf{S}_1). \quad (22)$$

This type of impurity may correspond to a charge island that is weakly coupled to a mesoscopic wire or to doping in a quasi-one dimensional compound where one atom in the chain has been substituted. We have recently considered this type of impurity in the context of doping in spin-1/2 compounds and as a simple experimental example of the two channel Kondo effect.⁹ In this section we analyze the induced density oscillations in more detail, especially in connection with the reflection coefficient.

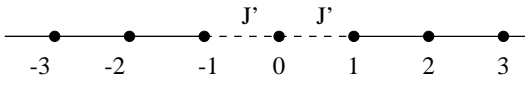


FIG. 5. Two modified links.

The model in Eq. (22) is equally simple as the one-link impurity, but the renormalization behavior is known to be quite different.⁷ Already for the non-interacting case at half filling the system shows a resonant behavior with perfect transmission $R = 0$, so that this corresponds to the simplest case of resonant tunneling considered by Kane and Fisher^{5,8} (at half-filling the impurity potential is automatically tuned to the resonant condition). With interactions $U \neq 0$ the reflection coefficient is no longer exactly zero, but shows nonetheless a renormalization to perfect transmission as $T \rightarrow 0$ in sharp contrast to the one-link impurity. This difference in renormalization behavior is easily explained by the different parity symmetry of the problem (namely site- instead of link-parity). For a small perturbation from a periodic chain $J' \sim J$ the leading operator is now *irrelevant* with scaling dimension of $d = 1 + g$, so that a perfectly transmitting chain is the stable fixed point. For small couplings $J' \gtrsim 0$ on the other hand, the leading perturbing operator is marginally relevant, and the situation is similar to the two channel Kondo effect where the two ends of the chain play the role of two independent channels.^{7,9}

Apart from the renormalization behavior there is another key difference between the one- and two-link impurities: In the two-link impurity model there is an “active” impurity site that carries a spin or charge degree of freedom, which in turn must be *screened* by the surrounding system. Therefore, the density oscillations are no longer simply determined by the backscattering in Eq. (12), but there is also a so-called screening cloud induced in the system. From perturbation theory in the leading irrelevant operator the functional dependence of this screening cloud can be calculated⁹ and the total alternating density χ^{alt} is a sum of two contributions

$$\chi^{\text{alt}}(x) = c_I (-1)^x \ln[\coth(xT)] - c_R (-1)^x \chi^{\text{bs}}(x), \quad (23)$$

where the first term is the induced screening cloud while the second term is the familiar contribution due to

backscattering in Eq. (12). Interestingly, the two contributions have opposite sign, so that the density oscillations vanish at a special distance from the impurity, but then increase again due to the backscattering contribution. This behavior is shown in Fig. 6 together with a fit to the two contributions in Eq. (23). The special distance at which the density oscillations vanish grows as we approach the stable fixed point ($J' \rightarrow J$ or $T \rightarrow 0$). As already with the one-link problem, we use again the numerical open chain data as a reference for χ^{bs} instead of the more simplified analytical form of the backscattering contribution in Eq. (12) since this minimizes the corrections due to irrelevant operators. However, even the analytical form in Eq. (12) gives very good fits, so that none of our findings are affected by this choice.

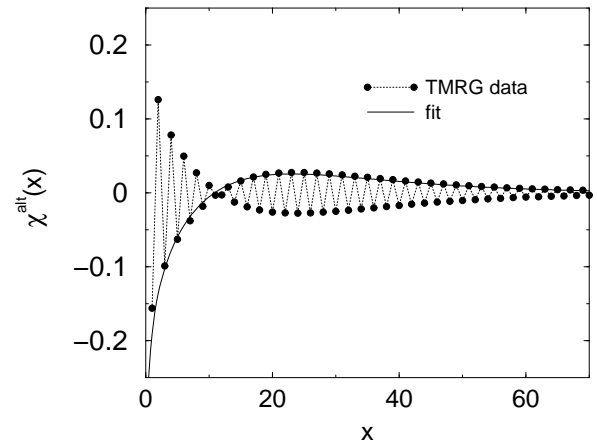


FIG. 6. Alternating part of the local susceptibility for the two-link impurity for $T/J = 0.04$ and $J'/J = 0.6$. Fit to Eq. (23).

It is now straightforward to extract the reflection coefficient from the numerical data with the help of Eq. (15) and Eq. (23) as shown in Fig. 7. Below a cross-over temperature T_K depending on J' the reflection coefficient clearly decreases and eventually approaches perfect transmission as $T \rightarrow 0$. Above T_K the renormalization of the reflection coefficient is rather weak and converges to a finite constant (never approaching complete reflection as the temperature increases).

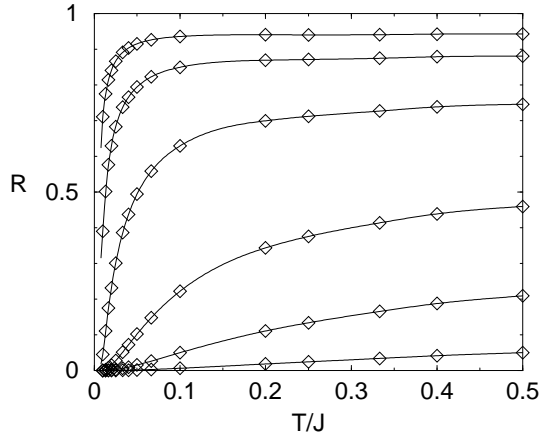


FIG. 7. Reflection coefficient R of the two-link impurity for $J'/J = 0.05, 0.1, 0.2, 0.4, 0.6, 0.8$ from above. The lines are guides for the eye.

Equally interesting is the induced screening cloud. In this case, the coefficient c_I approaches a constant as $T < T_K$ as it should, since this contribution was determined from perturbation theory around the stable fixed point. Above the cross-over temperature, however, this contribution vanishes quickly. This behavior is shown in Fig. 8: In general the behavior of the coefficient c_I vs. J' is temperature dependent and c_I increases as the temperature is lowered. However, as $T \ll T_K$ all curves approach a limiting value, which gives a universal behavior as a function of J' (thick line).

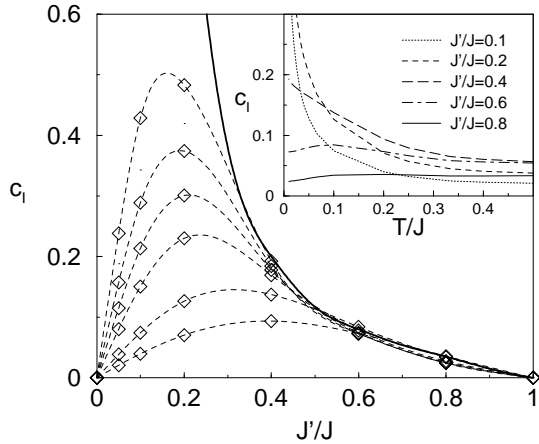


FIG. 8. Coefficient c_I vs J' of the two link impurity for different temperatures $T/J = 0.2, 0.1, 0.04, 0.025, 0.0167, 0.01$ from below. For $J' \approx J$ and/or low temperatures c_I approaches a universal T -independent curve (thick line). Inset: c_I vs T . The lines are guides for the eye.

The competing contributions in Eq. (23) have the opposite renormalization behavior: Above T_K backscattering is constant, while the screening cloud is reduced which is the open chain behavior. Below T_K on the other hand backscattering is reduced, while the coefficient for the induced screening cloud is constant, which is the be-

havior of the two channel Kondo fixed point. Note, that although the coefficient c_I is finite as $T \rightarrow 0$, the screening cloud itself diverges logarithmically with $-\ln(xT)$, which is a clear indication of the famous over-screening in the two channel Kondo effect. As we approach the unstable fixed point the order of limits becomes crucial: For zero coupling there is no screening cloud at all $\lim_{T \rightarrow 0} \lim_{J' \rightarrow 0} c_I = 0$, while for zero temperature the coefficient becomes infinite $\lim_{J' \rightarrow 0} \lim_{T \rightarrow 0} c_I = \infty$. Remarkably, exactly at zero temperature a minute perturbation therefore induces an infinite screening cloud, although this behavior occurs in an unphysical limit.

C. Impurity at the edge

Another category of impurities we can consider are imperfections near the end of a chain. In this case the boundary always gives complete backscattering, but as we will see the impurity can still give interesting effects on the density oscillations. The simplest case to consider is a modified link at the edge of a chain as depicted in Fig. 9. For the interacting case $U = 2t$ it is again useful to write the Hamiltonian in terms of the Heisenberg spin-chain model

$$H = J \sum_{i=1}^{\infty} \mathbf{S}_i \cdot \mathbf{S}_{i+1} + J' \mathbf{S}_0 \cdot \mathbf{S}_1. \quad (24)$$

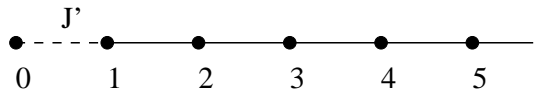


FIG. 9. Edge impurity.

Just like the two-link impurity was related to the two-channel Kondo problem, we can identify the field theory description of the edge impurity model with the regular one-channel Kondo problem. There are two possible fixed points: The case $J' = 0$ corresponds to the unstable fixed point of a decoupled spin at the end of a chain with a marginally relevant perturbation for $J' \gtrsim 0$. The case $J' = J$ corresponds to the completely screened spin, which is a stable fixed point with a leading irrelevant operator of scaling dimension $d = 2$. Just like in the ordinary Kondo effect both fixed points are represented by the same boundary condition and differ only by a simple $\pi/2$ phase shift on the fermions. (The infinite coupling fixed point $J' \rightarrow \infty$ is also stable, but is actually absolutely equivalent to the $J' = J$ fixed point since both cases represent a $\pi/2$ phase shift on the fermions by removing or adding a site, respectively). For intermediate couplings the phase shift Φ takes on values between 0 and $\pi/2$ which will be reflected in the backscattering contribution of the density oscillations as we will see below.

A screening cloud for the impurity spin at the end should also be present in this model, but with a different

behavior than for the overscreened case in Eq. (23). Instead we find that the leading operator that causes the screening cloud is the same as that for an edge magnetic field in the xxz-chain which has been analyzed in Ref. 25, so we can use the corresponding result for the shape of the induced screening cloud. Taking into account finite temperatures and the phase shift on the fermions we can write for the density oscillations

$$\chi^{\text{alt}}(x) = c_I \frac{(-1)^x \sqrt{T}}{\sqrt{\sinh(4xT)}} - \cos(\pi x + 2\Phi) c \chi^{\text{bs}}(x), \quad (25)$$

where the first term is the induced screening cloud, while the second term is the backscattering contribution in Eq. (12) but with a phase shift Φ . However, the coefficient c always takes the value corresponding to complete backscattering in Eq. (11). There is also an implied shift of $2\Phi/\pi$ in the argument of χ^{bs} , which we used for a self-consistent fitting. The effective boundary condition in the continuum limit is therefore technically between two lattice sites (although it is not really that meaningful to define locations on the scale of less than a lattice spacing in the continuum limit theory anyway).

Figure 10 shows the envelope of the alternating part of the susceptibility for temperature $T = 0.04J$ and different couplings J' , which always fits well to the superposition in Eq. (25). At the fixed points $J' = 0$ and $J' = J$ there is no screening, but the backscattering contribution has opposite signs due to the $\pi/2$ phase shift.

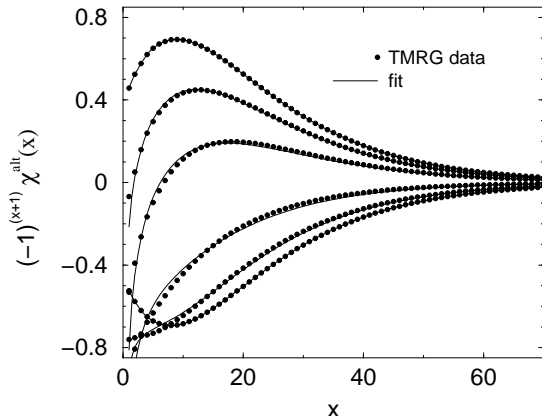


FIG. 10. Alternating susceptibility for the edge impurity at $T/J = 0.04$ for $J'/J = 0, 0.1, 0.2, 0.4, 0.6, 1.0$ from above. Fits to Eq. (25).

It is now straightforward to extract the screening cloud amplitude c_I and the phase shift Φ from our numerical data for all temperatures and couplings J' . As expected we find that the phase shift increases with J' and renormalizes to larger values as the temperature is lowered as shown in Fig. 11. In the limit of very low temperatures the jump to the stable fixed point value $\Phi = \pi/2$ becomes more abrupt as a function of J' .

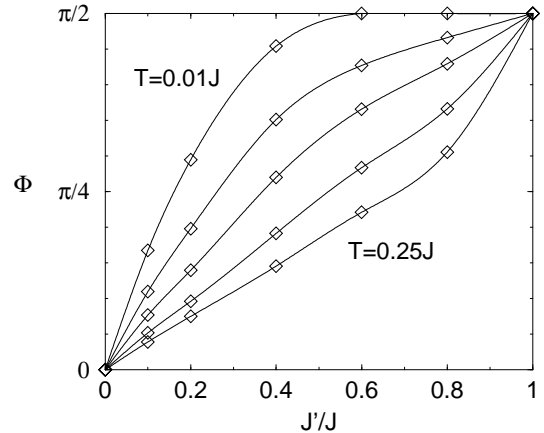


FIG. 11. Phase shift of alternating part of the edge impurity for $T/J = 0.25, 0.1, 0.04, 0.02, 0.01$ from below. The lines are guides for the eye.

The screening cloud coefficient c_I again approaches a constant as we lower the temperature below T_K as shown in Fig. 12. Although formally the behavior looks similar to the over-screened case of the two link problem in Fig. 8 it is important to realize that now the screening cloud in Eq. (25) is finite as $T \rightarrow 0$ and drops off with $1/x$ (while in the two link case the screening cloud was divergent with $\ln xT$).

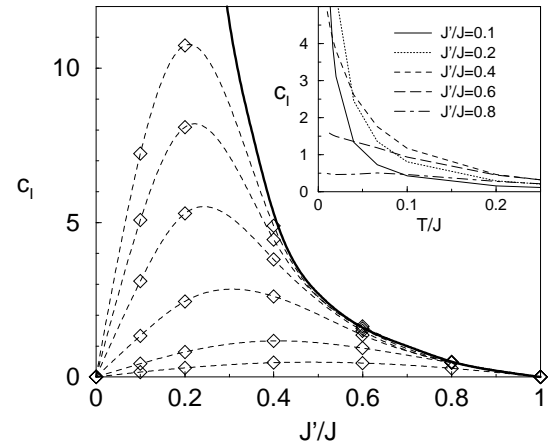


FIG. 12. Coefficient c_I vs. J' of the edge impurity for $T/J = 0.2, 0.1, 0.04, 0.02, 0.0133, 0.01$ from below. The lines are a guide for the eye.

D. Generalized two link impurity

It is now instructive to summarize the findings of the three impurity models in the previous subsections by considering one generalized two link impurity model that is *not symmetric* as shown in Fig. 13

$$H = J \sum_{i \neq -1, 0} \mathbf{S}_i \cdot \mathbf{S}_{i+1} + J_1 \mathbf{S}_{-1} \cdot \mathbf{S}_0 + J_2 \mathbf{S}_0 \cdot \mathbf{S}_1. \quad (26)$$

The three impurity cases above can be identified easily:

- $J_2 \neq J_1 = J$ one modified link in Eq. (19)
- $J_1 = J_2 \neq J$ two modified links in Eq. (22)
- $J_1 = 0, J_2 \neq J$ edge impurity in Eq. (24)

The density oscillations for the more general model in Eq. (26) are much more complex than in the special cases, so that a detailed analysis of this effect is not always useful. The renormalization behavior on the other hand is straightforward and can be read off from what we already know about the special cases.

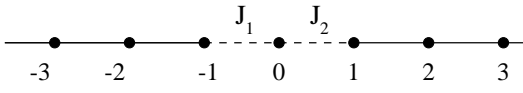


FIG. 13. Generalized two-link impurity.

A weak coupling $J_1 \gtrsim 0$ and $J_2 \gtrsim 0$ to an additional site is always marginally relevant, so that the open chain with a decoupled impurity site is unstable for any antiferromagnetic coupling (i.e. negative hopping probability). The periodic chain on the other hand is only stable for the special site-parity symmetric case $J_1 = J_2$, where the renormalization behavior is analogous to the two channel Kondo effect. In general, however, one of the two couplings is larger and renormalizes to unity, absorbing the spin. The smaller coupling is then irrelevant as in the one-weak problem, so that the stable fixed point is an open chain with an absorbed impurity site $J_1 = J, J_2 = 0$ (or $J_2 = J, J_1 = 0$) in most cases, except for a site-parity symmetric impurity or two ferromagnetic coupling constants. The complete renormalization flow is summarized in Fig. 14 where the possible fixed points are indicated by the black dots. In cases where the coupling diverges to infinity a singlet forms, and we can therefore again describe the system by one of the four finite fixed points in the figure. Interestingly, the more stable fixed points always have a lower ground state degeneracy, in accordance with the g-theorem.²⁶ The phase diagram in Fig. 14 is valid for all interaction strengths $0 < U \leq 2t$ as long as the system is half-filled.

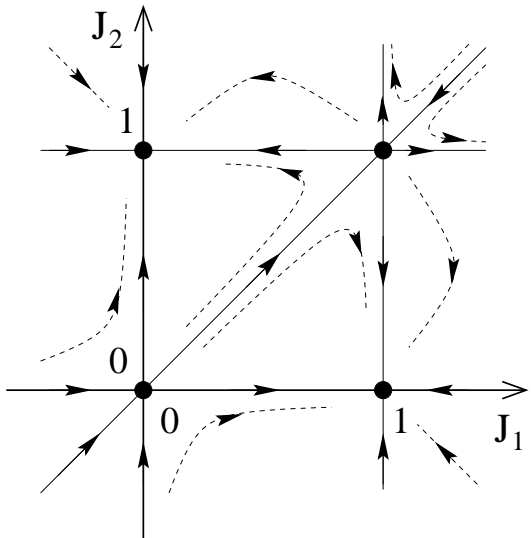


FIG. 14. Renormalization flow diagram.

E. Spin-1 impurity

We now turn to a magnetic impurity in the chain with spin $S_{\text{imp}} = 1$ given by the Heisenberg Hamiltonian

$$H = J \sum_{i \neq 0} \mathbf{S}_i \cdot \mathbf{S}_{i+1} + J' \mathbf{S}_{\text{imp}} \cdot (\mathbf{S}_0 + \mathbf{S}_1). \quad (27)$$

as shown in Fig. 15. In the previous impurity models in Sections III A-III D it was always possible to interpret the Heisenberg Hamiltonians equally well in terms of mesoscopic systems and electrons hopping on the lattice by identifying the spin-1/2 impurity in terms of an extra site or charge island. However, for the spin-1 impurity in Eq. (27) no meaningful interpretation in terms of spinless fermions is possible. On the other hand this impurity model has important implications for doping in quasi one-dimensional spin-1/2 compounds, so that we find it useful to discuss it here.

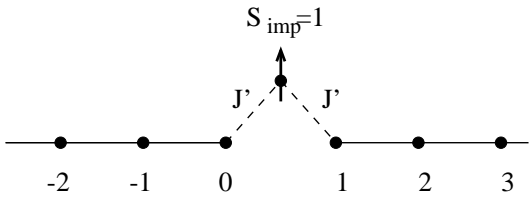


FIG. 15. The spin-1 impurity.

Similar to the impurity models in Sections III B and III C we find again that the field theory language is analogous to a Kondo impurity model. The two ends of the spin-chain play the role of the two channels coupled to a spin-1 impurity. A small antiferromagnetic coupling is therefore marginally relevant and the renormalization flow goes to the strong coupling limit. The stable fixed point is given by an open spin chain with two sites re-

moved and a decoupled singlet containing the spin-1 and the two end spins ($J' \rightarrow \infty$).

Just like the edge impurity in Sec. III C this Kondo-type model is an exactly screened impurity. The shape of the screening cloud is again given by that of an edge magnetic field²⁵ just like in Eq. (25)

$$\chi^{\text{alt}}(x) = c_I \frac{(-1)^x \sqrt{T}}{\sqrt{\sinh(4xT)}} - c_R (-1)^x \chi^{\text{bs}}(x), \quad (28)$$

where the first term is again the induced screening cloud, while the second term is the backscattering contribution in Eq. (12). As shown in Fig. 16 the fits to this expression are excellent (again using the open chain data as a reference for χ^{bs}). The coefficient c_I for the induced screening cloud again approaches a constant for temperatures below T_K which results in a universal curve as $T \rightarrow 0$ as shown in Fig. 17. The backscattering coefficient is an indication of the effective phase shift and changes sign depending on the temperature and coupling strength. From Fig. 16 it is clear that the backscattering coefficient c_R is positive for small coupling strengths J' (or equivalently high temperatures) and negative for larger coupling strengths J' (or equivalently lower temperatures). The renormalization of c_R is explicitly shown in the inset of Fig. 17. As $T \rightarrow 0$ the jump of c_R to negative values happens at smaller J' and becomes very sharp.

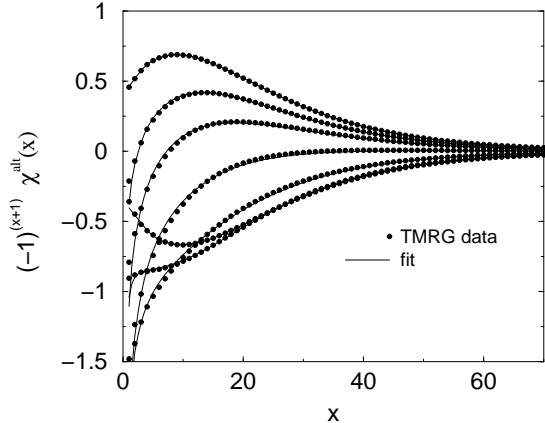


FIG. 16. Envelope of alternating part at $T/J = 0.04$ for the spin-1 impurity. From above at $x \gtrsim 20$: $J'/J = 0, 0.05, 0.1, 0.2, 0.4, 4.0$. Fits to Eq. (28).

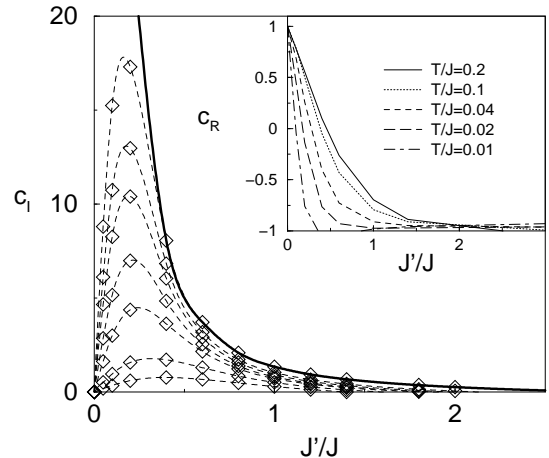


FIG. 17. Coefficient c_I of the spin-1 impurity for $T/J = 0.2, 0.1, 0.04, 0.025, 0.0167, 0.0133, 0.01$ from below. Inset: Backscattering coefficient c_R . The dashed lines are a guide for the eye.

More interesting are the experimental consequences for Knight shift experiments in doped spin-1/2 chain compounds (as for example Ni doping in CuO chains). For that case we can predict an interesting NMR spectrum with a characteristic feature (sharp edge) corresponding to the maximum in the alternating susceptibility. Such a sharp edge has been observed before in NMR experiments on spin-1/2 chain compounds with non-magnetic defects.²² In that case the sharp edge broadens with a $1/\sqrt{T}$ behavior as discussed in Sec. II. For the magnetic spin-1 impurities a sharp edge from the maximum in the backscattering part may also be present, but it depends on if the temperature is above or below T_K how this feature changes. Above T_K the backscattering part becomes weaker as the temperature is lowered, but the induced screening cloud increases, so that the sharp kink may vanish in a quickly broadening line-shape from the screening cloud as shown in the left part of Fig. 18. Below T_K on the other hand, the screening has saturated and the backscattering contribution dominates again (albeit with a phase shift). Therefore, the kink feature in the NMR spectrum will sharpen further as the temperature is lowered and widen with the usual $1/\sqrt{T}$ behavior as shown in the right part of Fig. 18. The detailed T -dependence can be predicted for any particular value of J' of an actual experimental compound.

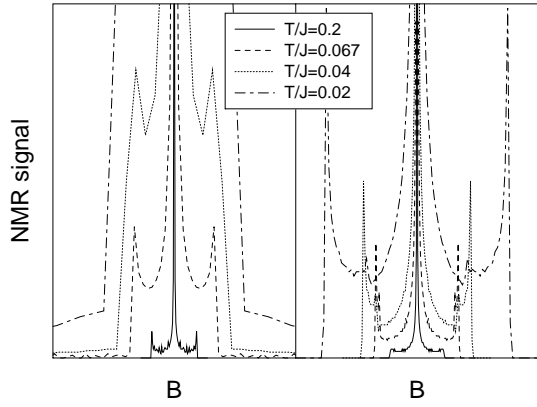


FIG. 18. NMR signal of the spin-1 impurity for $J'/J = 0.1$ (left) and $J'/J = 1.4$ (right).

F. Integrable impurity model

Finally, we would like to consider a more exotic impurity model which has been especially constructed to preserve the integrability of the entire system.²⁷ We consider here the simplest non-trivial example of such an impurity model which corresponds to an impurity spin with $S_{\text{imp}} = 1$ that is coupled in a special way to two sites in the chain. The corresponding Hamiltonian has been set up in Ref. 27

$$H = J \sum_{i \neq 0} \mathbf{S}_i \cdot \mathbf{S}_{i+1} - \frac{7J}{9} \mathbf{S}_0 \cdot \mathbf{S}_1 + \frac{4J}{9} [(\mathbf{S}_0 + \mathbf{S}_1) \cdot \mathbf{S}_{\text{imp}} + \{\mathbf{S}_0 \cdot \mathbf{S}_{\text{imp}}, \mathbf{S}_1 \cdot \mathbf{S}_{\text{imp}}\}], \quad (29)$$

where \mathbf{S}_{imp} is the external spin-1 impurity and $\{\cdot, \cdot\}$ denotes the anticommutator.

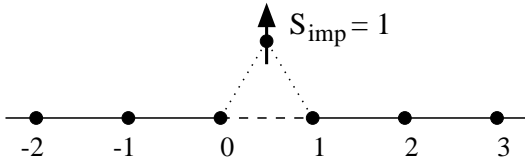


FIG. 19. The integrable impurity.

A closer analysis of this model²⁸ showed that the thermodynamics at low temperatures were in fact described by a *periodic* spin chain with one additional site and an asymptotically free impurity spin with $S = 1/2$, so that it appears that the original spin-1 has somehow been partially absorbed by the chain. From a field theory point of view it was later shown that this type of impurity corresponds in fact to an unstable fixed point which can only be reached by an artificial tuning of the coupling parameters.²⁹

We are now interested in what kind of density oscillations might be observable from such an impurity. Interestingly, we found that the density oscillations were *identically zero at all temperatures* as if the system was translationally invariant. The impurity Hamiltonian in

Eq. (29) was of course constructed in a way to avoid all backscattering, but it is remarkable that even the induced alternating part from the magnetic impurity vanishes exactly, i.e. no conventional screening takes place.

Nonetheless, the impurity spin is somehow reduced from a spin-1 to an effective spin-1/2 as the temperature is lowered. This can be explicitly seen from the impurity susceptibility in small magnetic fields

$$\langle S_{\text{imp}}^z \rangle = B \frac{C_{\text{Curie}}}{T} \quad (30)$$

where we have assumed some type of Curie-law. At high temperatures the impurity susceptibility must follow the Curie-law for a spin-1 $C_{\text{Curie}} = 2/3$, while at low temperatures a Curie-law for a spin-1/2 $C_{\text{Curie}} = 1/4$ has been predicted up to logarithmic corrections.²⁸ In Fig. 20 we plot the temperature dependent Curie constant (i.e. the impurity susceptibility times temperature). It appears that the asymptotic value $C_{\text{Curie}} = 1/4$ is indeed approached with logarithmic corrections as $T \rightarrow 0$. The fit in the figure is

$$C_{\text{Curie}} = \frac{1}{4} + \frac{1}{8 \ln(2\pi/T)} + a \frac{\ln(\ln(2\pi/T)/b)}{\ln(2\pi/T)^2} \quad (31)$$

with $a = 1.62$ and $b = 1.32$.

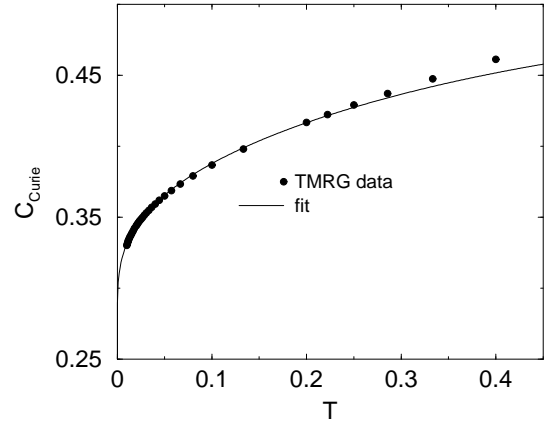


FIG. 20. Susceptibility of the spin-1 in the integrable model multiplied by temperature. Fit to Eq. (31).

IV. NUMERICAL METHOD

The numerical method we have used here is based on the Density Matrix Renormalization Group (DMRG)³⁰ applied to transfer matrices. While the ordinary DMRG considers the properties of individual eigenstates in a finite system, we are interested in the thermodynamic limit, namely properties of an infinite system at finite temperatures. This can be achieved by the Transfer Matrix Renormalization Group (TMRG),¹² which we adapted especially for impurities^{9,11} as we will review briefly. We consider the partition function Z of the models in Eqs. (1) and (2). After the standard Trotter decomposition, we obtain for an infinite system ($L \rightarrow \infty$)

$$Z = \lim_{M \rightarrow \infty} \text{tr} T_M^{L/2} \rightarrow \lim_{M \rightarrow \infty} \lambda_M^{L/2}, \quad (32)$$

where T_M is the transfer matrix with M time-slices. In the limit of infinite system size only the largest eigenvalue λ_M determines the thermodynamics of the system, which we find numerically. We start with small time-steps so that the Trotter-error is negligible, and successively increase the number of time-slices M to reach lower temperatures. At each step the dimension of T_M increases so we keep only the most important states to describe the state with the highest eigenvalue λ_M by using the DMRG algorithm with some modifications for asymmetric matrices.¹¹ A measurement of the local spin-density at site j for example is straightforward, since we can just absorb the measuring operator S_j^z into one of the transfer matrices $T_M \rightarrow T_M^{sz}$

$$\langle S_j^z \rangle = \frac{1}{Z} \text{tr} S_j^z e^{-\beta H} \rightarrow \frac{\langle \psi_M | T_M^{sz}(j) | \psi_M \rangle}{\lambda_M}, \quad (33)$$

where $\langle \psi_M |$ and $| \psi_M \rangle$ are the left and right target states for the eigenvalue λ_M . So far we have considered a translational invariant system.

We now introduce a generic impurity which modifies one of the transfer matrices $T_M \rightarrow T_{\text{imp}}$. Even in the presence of impurities the thermodynamics of the system is entirely determined by the highest eigenvalue λ_M and corresponding eigenstate of the pure transfer matrix T_M which always appears with an infinite power in the partition function in Eq. (32). The measurement of the spin (or charge) density near the impurity is again straightforward. For the spin density at a distance of j sites from the impurity we write

$$\langle S_j^z \rangle = \frac{\langle \psi_M | T_M^{sz} (T_M)^{j/2} T_{\text{imp}} | \psi_M \rangle}{\lambda_M^{j/2+1} \langle \psi_M | T_{\text{imp}} | \psi_M \rangle}. \quad (34)$$

Since we step-wise approximate the transfer matrix, it is important to make a careful error-analysis. The error due to the Trotter approximation is the simplest to estimate since it is just proportional to the square of the time-step $\tau = 1/TM$. We found that a value of $\tau = 0.05/J$ makes this error negligible compared to the DMRG truncation errors. To estimate the truncation errors we can compare our results to the exact solution of the free fermion Hamiltonian in Eq. (1) with $U = 0$. The structure of the transfer matrix is not fundamentally changed by taking $U = 0$ so that the truncation error will be of the same order as for $U \neq 0$. Keeping 64 states we find for the local response of the spins closest to typical impurities a relative error of less than 10^{-4} for $T > 0.04$, less than 10^{-3} for $0.02 < T < 0.04$ and a relative error of less than 10^{-2} for temperatures $0.01 < T < 0.02$. However, already from Eq. (34) it is clear that the spin and charge densities far away from the impurity will contain a larger error. Each transfer matrix contains a small error ϵ which then gets exponentiated in Eq. (34) and hence the oscillating part of the density $\langle S_j^z \rangle$ is suppressed exponentially with distance j

$$\langle S_j^z \rangle_{\text{osc}} \propto (1 - \epsilon)^j = \exp(-j\epsilon) \quad (35)$$

where ϵ depends only on temperature. This exponential suppression with the distance from the boundary is again a consequence of the fact that the incoming and outgoing waves lose coherence but this time due to error fluctuations. However, the corresponding energy scale from the truncation error is always smaller than the temperature in our case. We observe that the suppression error in Eq. (35) is actually very systematic, so that we can even correct our data very well using Eq. (35). For free fermions we find to high accuracy the following dependence of the error on temperature

$$\epsilon = 0.06 \exp(-58T), \quad (36)$$

where we have kept 64 states in the TMRG simulations. For interacting fermions the suppression also has the exponential dependence in Eq. (35), but the energy scale ϵ is in general dependent on the interaction U . For the Heisenberg model an independent analysis of the free energy hinted at a value of approximately $\epsilon = 0.02 \exp(-34T)$, but the value in Eq. (36) is more reliable and gives a relatively good estimate of the error for all interaction strengths. We chose to correct our data for the alternating fermion densities by dividing out the factor in Eq. (35) together with the estimate in Eq. (36) in all cases presented above. However, the use of this correction or the particular choice of the error ϵ makes no qualitative difference in any of our findings, since the temperature suppression always dominates (i.e. the energy scale in Eq. (36) is always smaller than the temperature). Another important energy scale is the finite magnetic field B that is used in the simulations (i.e. how close the system is to half filling). We typically used a value of $B = 0.003$ which makes the magnetic length scale in Eq. (10) always negligible compared to the finite temperature correlation length.

V. CONCLUSION

We have considered a number of impurity models and were able to extract detailed information about the backscattering amplitude, the backscattering phase-shift, and the impurity screening effects by examining the Friedel oscillations. The results for the various impurities have direct and indirect implications for a large number of theoretical models and experimental systems as we will summarize below.

A. Kondo-type impurities

Kondo impurity problems are maybe the most famous examples of impurity renormalization effects ever since the classic work by Wilson.³¹ Many of the impurity models we have considered here are analogous to Kondo impurity problems in terms of the field theory language.

In particular, the field theory description of a Heisenberg chain is the same as that of the spin-channel for a spin-full electron field (while the charge excitations are neglected). Moreover, it is known that coupling the open end of a Heisenberg chain to an impurity spin produces the same impurity operators as in the real Kondo problem.^{7,32} The number of channels in the equivalent Kondo problems is given by the open ends that the impurity spin is connected to (e.g. the two link impurity in Sec. III B is analogous to the two channel S=1/2 Kondo problem). It is important to realize that the Heisenberg spins in the chains that we consider here have different expressions in terms of the boson fields than the real electron spins in the full three dimensional Kondo problems. Nonetheless, we can still use our models to gain some insight into the central aspects of renormalization, scaling, cross-over temperature, and screening clouds.

We have shown that the Kondo-type impurities indeed show the expected renormalization to a screened impurity spin. In particular, we have found a diverging screening cloud (and vanishing backscattering) for the over-screened case in Sec. III B, while the exactly screened cases in Sec. III C and III E are characterized by a finite screening cloud and a phase shift in the backscattering as $T \rightarrow 0$.

To analyze the renormalization process more quantitatively it is important to introduce the concept of scaling. It can be expected that the impurity introduces a new energy scale that depends on the initial bare coupling constants. Commonly this energy scale is referred to as the cross-over temperature T_K . By making use of scale invariance it is then possible to describe the renormalization process universally in terms of the single parameter T/T_K . In particular, impurity properties like the impurity susceptibility are described by a universal scaling function $\chi_{\text{imp}} = f(T/T_K)/T$, which is valid for all T and T_K below the cut-off. This behavior was demonstrated explicitly before for the two weak link problem⁹ and works for all Kondo-type impurities in this paper (not shown). In fact it is possible to extract the cross-over temperature T_K up to an arbitrary overall scale explicitly by collapsing the data according to the scaling analysis.^{9,11} We have determined T_K this way as a function of coupling J' in each case as shown in Fig. 21 (up to an arbitrary overall scale). The Kondo temperature shows the same exponential dependence for small J'

$$T_K \propto \exp(-0.85J/J') \quad (37)$$

as shown in Fig. 21 (coming from the same marginally relevant operator at the unstable fixed point in all cases). The underscreened case of a spin-1 coupled to the end of one chain has also been included in Fig. 21 for completeness.

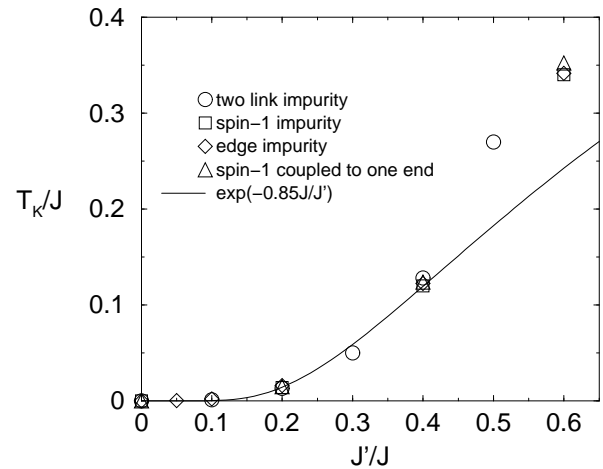


FIG. 21. Crossover temperature T_K of four different Kondo-type impurities. T_K has been multiplied by arbitrary constants in order to compare the four cases.

More interesting in the context of the density oscillations is maybe the scaling of the screening cloud. As the screening cloud we define that part of the alternating density that is induced by the magnetic impurity, labeled by c_I in Eqs. (23), (25), and (28). In Ref. 4 it was postulated that the screening cloud in the real Kondo effect should be a function of the scaling variables xT and T/T_K . In our cases we can make a similar argument except that we need to include an overall factor T^{g-1} to account for the dimensionality of the correlation functions. We therefore obtain the following scaling law

$$\chi^{\text{screening}} = T^{g-1} f(xT, T/T_K). \quad (38)$$

Indeed we find that the shape of the screening cloud is not affected by T_K and can always be expressed as a function of the scaling variable xT . The coefficient c_I must therefore be a function of T/T_K multiplied by appropriate powers of T . As an example we can take the two link problem at $g = 1/2$ with the screening cloud given in Eq. (23), where the coefficient can be written as $c_I = f(T_K/T)/\sqrt{T}$ with some function f . In Fig. 22 we replot the coefficient c_I analogous to Fig. 8 but with the argument replaced by T_K/T instead of J' . The inset shows that the data indeed collapses if multiplied by \sqrt{T} as implied by Eq. (38). The solid line in Fig. 8 therefore is proportional to $1/\sqrt{T_K}$ and diverges exponentially with J' according to Eq. (37). Similar arguments can be made for the coefficients c_I in the screening clouds of the exactly screened cases in Eqs. (25) and (28), except that $c_I = f(T_K/T)/T$ and the solid line is proportional to $1/T_K$ in that case.

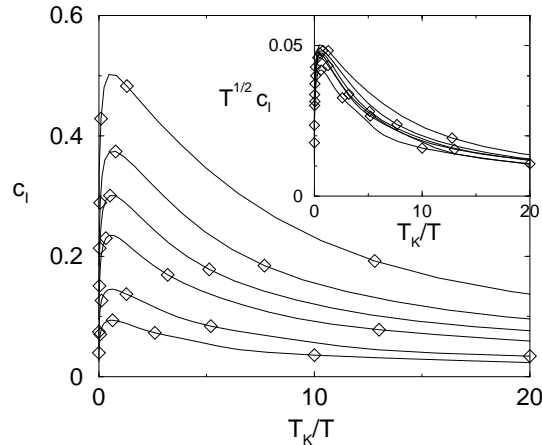


FIG. 22. The coefficient c_I for the two link impurity in Eq. (23) as a function of T_K/T for different temperatures $T/J = 0.2, 0.1, 0.04, 0.025, 0.0167, 0.01$ from below.

B. Doping in spin chains

Our results also have immediate experimental consequences for impurities in spin-chain compounds such as KCuF_3 or Sr_2CuO_3 . The spin density oscillations are directly linked to the local Knight shifts (susceptibilities) close to the corresponding impurities, which can be measured by standard NMR techniques or muon spin resonance. NMR experiments have already successfully detected the sharp feature corresponding to the maximum in Fig. 1 from open boundaries due to non-magnetic defects that were naturally present in the crystal.²² We now propose to use intentional doping with magnetic or non-magnetic impurities to see the predicted renormalization effects. Impurities of one or two modified links in the chain can possibly be created by doping the surrounding non-magnetic atoms in the crystal at link or site parity symmetric locations. The spin-1 impurities in Sec. III E could be produced in a more straightforward way by substituting Cu ions by Ni ions in the corresponding compounds. In Sec. III E we discussed explicitly how the renormalization effects for spin-1 impurities would show up in an actual experiment. Similar arguments can also be made for the two link⁹ or one link impurities by simply using the analytic form of the corresponding alternating spin densities with the coefficients c_R and c_I that we have calculated.

In general we find a strong enhancement of the antiferromagnetic order near impurities. This enhancement can also be observed in higher dimensions² and may have important consequences for impurity-impurity interactions. In one dimension this effect is strongest, but the complex functional dependence we found here is often beyond the intuitive explanation in terms of valence bond states.²

C. Impurities in Mesoscopic systems

Finally, our analysis also allows us to draw important conclusions for transport measurements in one dimensional mesoscopic structures. This is probably the first time that the conductivity could be explicitly extracted from numerical data for Luttinger Liquid type models. Not surprisingly, we found that a generic impurity indeed renormalizes to complete backscattering as the temperature is lowered, and we also could explicitly observe the “healing effect” in the symmetric resonant tunneling case as predicted by Kane and Fisher.^{1,5,8} Our numerical results not only confirm the asymptotic power-laws, but also give a quantitative estimate of the conductivity for all temperatures and impurity strengths. For a generic impurity with little or intermediate backscattering we find that the asymptotic scaling region turns out to be extremely narrow. For impurities with strong backscattering we find that the conductivity is *enhanced* by interactions at higher temperatures.

One obvious question is how those results can be generalized to spinful electron systems and carbon nanotubes. A number of works have addressed the question of impurities in spinful wires^{5,6,33,34} and found a richer structure since renormalization takes place in both the spin and the charge channels. However, if realistic SU(2) invariant interactions are assumed the generic behavior is very similar to the spinless case, so that we expect that our results for the reflection coefficient carry over in a straight forward fashion. The shape and amplitude of the density oscillations, however, will in general be very different for spinful electron systems. For carbon nanotubes it has been shown that the Friedel oscillations impose a characteristic pattern that can be observed with scanning tunneling microscopy.³⁵ For spinful wires it is expected that the Friedel oscillations from an open end can reveal the nature of the spin-charge separation in real space.³⁶ Although our results do not allow for quantitative predictions of the density oscillations in spinful systems, we generally expect that strong, long-range density oscillations should be present from backscattering in one-dimension. One experimental consequence of those oscillations is that the measurement through a lead close to an impurity is very sensitive to the exact location. Previous studies have shown that even the distance between two leads can play a crucial role.³⁷ The current may be strongly enhanced or depleted, depending on if the distance to the impurity is a multiple of $2k_Fx$ or not. Especially interesting are therefore experiments with an adjustable lead such as a tunneling tip. The direct observation of those oscillations could give detailed information about both the nature of the impurity and also about the interactions in the system.

ACKNOWLEDGMENTS

S.R. acknowledges support from the Swedish Foundation for International Cooperation in Research and Higher Education (STINT). S.E. is thankful for the support from the Swedish Natural Science Research Council through the research grants F-AA/FU 12288-301 and S-AA/FO 12288-302.

-
- ¹ C.L. Kane and M.P.A. Fisher, Phys. Rev. Lett. **68**, 1220 (1992).
- ² G.B. Martins, M. Markus J. Riera and E. Dagotto, Phys. Rev. Lett. **78**, 3563 (1997).
- ³ J. Friedel, Nuovo Cimento Suppl. **7**, 187 (1958).
- ⁴ E.S. Sørensen and I. Affleck, Phys. Rev. B **53**, 9153 (1996).
- ⁵ C.L. Kane and M.P.A. Fisher, Phys. Rev. B **46**, 15233 (1992).
- ⁶ K.A. Matveev, D.X. Yue and L.I. Glazman, Phys. Rev. Lett. **71**, 3351 (1993); D.X. Yue, L.I. Glazman and K.A. Matveev, Phys. Rev. B **49**, 1966 (1994).
- ⁷ S. Eggert and I. Affleck, Phys. Rev. B **46**, 10866 (1992).
- ⁸ C.L. Kane and M.P.A. Fisher, Phys. Rev. B **46**, 7268 (1992).
- ⁹ S. Eggert and S. Rommer, Phys. Rev. Lett. **81**, 1690 (1998); Physica B **261**, 200 (1999).
- ¹⁰ S.J. Qin, M. Fabrizio and L. Yu, Phys. Rev. B **54**, R9643 (1996); S.J. Qin, M. Fabrizio, L. Yu, M. Oshikawa and I. Affleck, Phys. Rev. B **56**, 9766 (1997).
- ¹¹ S. Rommer and S. Eggert, Phys. Rev. B **59**, 6301 (1999).
- ¹² R.J. Bursill, T. Xiang and G.A. Gehring, J. Phys. C **8**, L583 (1996); X.Q. Wang and T. Xiang, Phys. Rev. B **56**, 5061 (1997); N. Shibata, J. Phys. Soc. Jpn. **66**, 2221 (1997).
- ¹³ N.M. Bogoliubov, A.G. Izergin and V.E. Korepin, Nucl. Phys. B **275**, 687 (1986).
- ¹⁴ A.E. Mattsson, S. Eggert and H. Johannesson, Phys. Rev. B **56**, 15615 (1997).
- ¹⁵ S. Eggert, H. Johannesson and A. Mattsson, Phys. Rev. Lett. **76**, 1505 (1996).
- ¹⁶ M. Fabrizio and A.O. Gogolin, Phys. Rev. B **51**, 17827 (1995).
- ¹⁷ S. Eggert and I. Affleck, Phys. Rev. Lett. **75**, 934 (1995).
- ¹⁸ S. Eggert, A.E. Mattsson and J.M. Kinaret, Phys. Rev. B **56**, R15537 (1997).
- ¹⁹ R. Egger and H. Grabert, Phys. Rev. Lett. **75**, 3505 (1995).
- ²⁰ S. Eggert, I. Affleck and M. Takahashi, Phys. Rev. Lett. **73**, 332 (1994).
- ²¹ V. Brunel, M. Bocquet and Th. Jolicœur, Phys. Rev. Lett. **83** 2821 (1999); I. Affleck and S.J. Qin, J. Phys. A: Math. Gen. **32**, 7815 (1999).
- ²² M. Takigawa, N. Motoyama, H. Eisaki and S. Uchida, Phys. Rev. B **55**, 14129 (1997); Phys. Rev. Lett. **76**, 4612 (1996); N. Fujiwara, H. Yasuoka, M. Isobe and Y. Ueda, Phys. Rev. B **58**, 11134 (1998).
- ²³ M. Laukamp, G.B. Martins, C. Gazza, A.L. Malvezzi, E. Dagotto, P.M. Hansen, A.C. Lopez and J. Riera, Phys. Rev. B **57**, 10755 (1998).
- ²⁴ M. Nishino, H. Onishi, P. Roos, K. Yamaguchi and S. Miyashita, Phys. Rev. B **61**, 4033 (2000).
- ²⁵ I. Affleck, J. Phys. A **31**, 2761 (1998).
- ²⁶ I. Affleck and A.W.W. Ludwig, Phys. Rev. Lett. **67**, 161 (1991).
- ²⁷ N. Andrei and H. Johannesson, Phys. Lett. **100A**, 108 (1984)
- ²⁸ P. Schlottmann, J. Phys. Condens. Matter **3**, 6617 (1991)
- ²⁹ E.S. Sørensen, S. Eggert and I. Affleck, J. Phys. A **26**, 6757 (1993).
- ³⁰ S.R. White, Phys. Rev. Lett. **69**, 2863 (1992); Phys. Rev. B **48**, 10345 (1993).
- ³¹ K.G. Wilson, Rev. Mod. Phys. **47**, 773 (1975).
- ³² I. Affleck, Acta Physica Polonica B **26**, 1869 (1995); preprint cond-mat/9512099.
- ³³ A. Furusaki and N. Nagaosa, Phys. Rev. B **47**, 4631 (1993).
- ³⁴ E. Wong and I. Affleck Nucl. Phys. B **417**, 403 (1994).
- ³⁵ C.L. Kane and E.J. Mele, Phys. Rev. B **59**, 12759 (1999); W. Clauss, D.J. Bergeron, M. Freitag, C.L. Kane, E.J. Mele and A.T. Johnson, Europhys. Lett. **47**, 601 (1999).
- ³⁶ S. Eggert, Phys. Rev. Lett. **84**, 4413 (2000).
- ³⁷ J.M. Kinaret, M. Jonson, R.I. Shekter and S. Eggert, Phys. Rev. B **57**, 3777 (1998); Physica E **1**, 265 (1997).